EUROPEAN JOURNAL OF MATERIALS SCIENCE AND ENGINEERING
Volume 3, Issue 4, 2018: 203-218 | www.ejmse.tuiasi.ro | ISSN: 2537-4338

ADDITIVE MANUFACTURED ALUMINUM ALLOY: MICROSTRUCTURE CHARACTERIZATION AS A FUNCTION OF ENERGY DENSITY

Luke SUTTEY*, Vadiraja SUDHAKAR

Montana Technological University, Butte, MT 59701, USA.

Abstract

In this investigation, detailed microstructural studies were performed to determine their influence on process parameters used in additive manufacturing of AlSi10Mg alloy. As-built specimen orientations and energy densities were the variable process parameters used to evaluate their influence on the resulting microstructures. Microstructures were characterized using a light microscope attached with a software for detailed analysis. Results revealed optimal microstructures for specimens produced with 45.4 J/mm^3 global energy density showing cellular-dendritic microstructures. Specimens with global energy density of 37.1 J/mm^3 produced an undesirable microstructure with relatively large melt pool boundaries.

Keywords: *microstructure, laser powder bed fusion (LPBF), $AlSi_{10}Mg$ alloy, build angle.*

Introduction

Aluminum alloys have an excellent combination of physical and mechanical properties that make them useful for varieties of engineering applications [1-3]. The melting practice for aluminum alloys can be varied to obtain microstructures to target the required static and dynamic properties desired in products [4, 5]. The coarse grain structures in aluminum alloys usually result in poor mechanical properties, due to slow cooling rates [2]. Additive manufactured aluminum alloy components are known to produce very fine microstructures contributing to improved mechanical properties [6]. Additive manufacturing of aluminum alloys is very complex as a result of its various inherent characteristics leading to potential defects in the final product. Many of the investigators [7, 8] were able to produce aluminum components with relatively fewer defects by choosing appropriate process parameters during additive manufacturing.

The aluminum alloy used in this study has a near eutectic composition (12.5% Si) having varieties of engineering applications. Various investigators [9-22] have studied the microstructural effects of laser additive processed aluminum-silicon alloy, but the detailed specific analysis on microstructural constituents is limited. The aim of this study is therefore to characterize and provide detailed analysis for the microstructures of additive manufactured AlSi10Mg alloy as a function of energy densities.

Experimental Procedure

Aluminum Alloy Powder and Additive Manufacturing Process

Aluminum alloy powder that was used for producing as-built test specimens had an average particle size of about 20 to 25 µm. During laser additive manufacturing (LAM) process,

*) Corresponding author: kvsudhakar@mtech.edu

the powder bed is created that rests on the build platform usually in a protective chamber, like in an argon gas atmosphere. Using the laser energy, the surface of the bed is heated that locally melts and fuses the powder in areas where solid metal is desired. After each laser exposure, another set of powders are brought-in and more as-built test specimens are produced.

Process Variables

Different energy density values at 37.1 J/mm^3, 45.4 J/mm^3, and 49.9 J/mm^3, were used in this investigation resulting from suitably varying appropriate LAM processing variables. The energy density was calculated using the following equation;

$$\psi = \frac{P}{vht} \quad (1)$$

Where, P = Power in Watt, v = laser scan speed in mm/s, h = hatch spacing in mm, and t = thickness in mm, of each layer of powder.

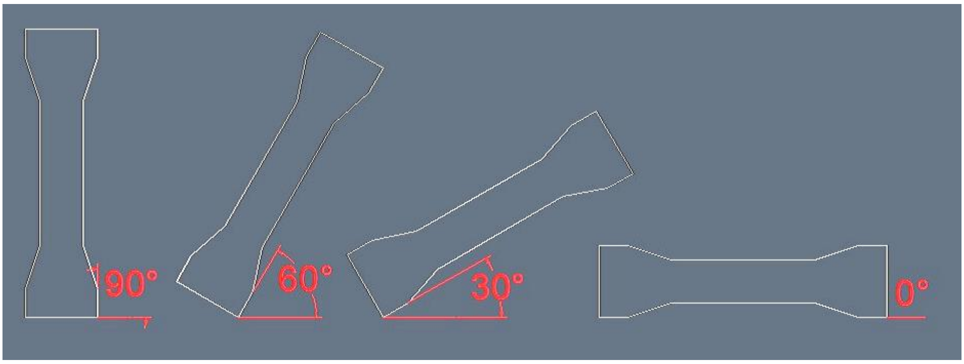

Fig. 1. Schematics of various specimen build angle orientations

The schematics of as-built specimen angle orientations are shown in Fig. 1.

Analysis of Microstructures

Austenitic stainless steel specimens were etched using (separately); Kalling's reagent and Villella's reagent. LEICA DM750M optical microscope was used to investigate microstructures.

Results and Discussion

Influence of Global Energy Density (GED) on Microstructure

Energy density at 49.9 J/mm^3

Fig. 2 shows the evidence of porosity, a solidification defect. Fig. 3 reveals a columnar structure with a limited heat affected zone, but lots of porosity.

Fig. 4 shows the microstructure of the specimens with 30° orientation demonstrating a structure with relatively fewer solidification defects. Fig. 5 shows the microstructure at another location that exhibits a columnar morphology with dendritic features.

Fig. 6 and 7 show microstructures of the specimen with 45^0 orientation with a coarse microstructure because of relatively slower rate of cooling. The porosity was minimal but showing a larger columnar structure.

The microstructure with melt pool boundaries and columnar structure with porosity, built at 60° orientation, are shown in Fig. 8 and 9, respectively. It may be seen in these figures that the columnar structure and the porosity are relatively smaller or finer.

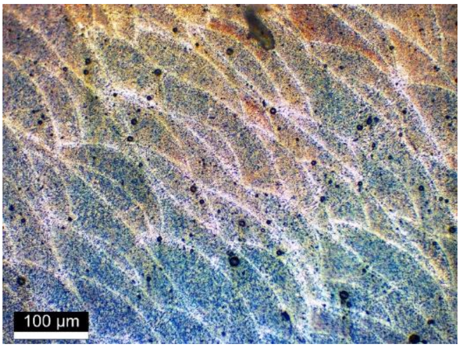

Fig. 2. Microstructure of a specimen with energy density, 49.9 J/mm^3 and 0° orientation

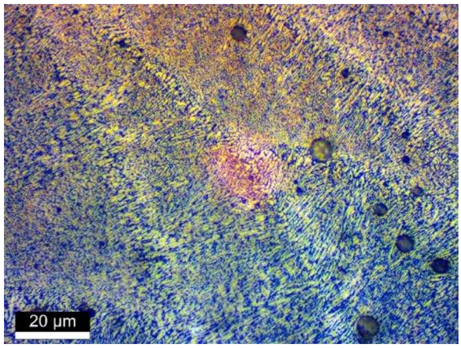

Fig. 3. Microstructure of a specimen shown in Fig. 2, revealing porosity and columnar structure

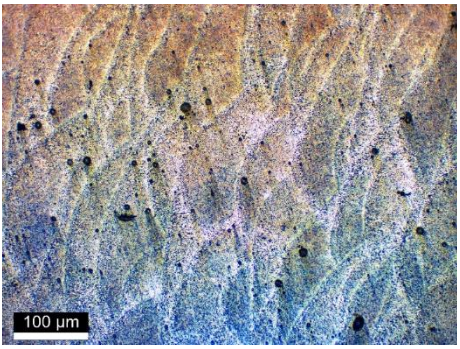

Fig. 4. Microstructure of a specimen with energy density, 49.9 J/mm^3 and 30° orientation

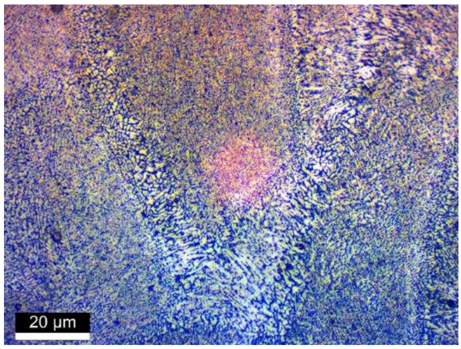

Fig. 5. Microstructure of a specimen shown in Fig. 4, showing columnar structure

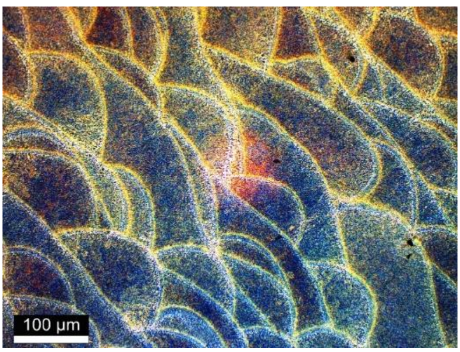

Fig. 6. Microstructure of a specimen with energy density, 49.9 J/mm^3 and 45° orientation

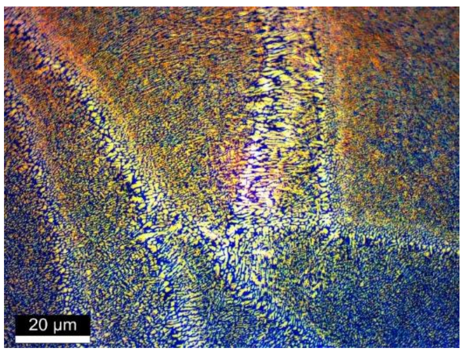

Fig. 7. Microstructure of a specimen shown in Fig. 6, showing columnar structure

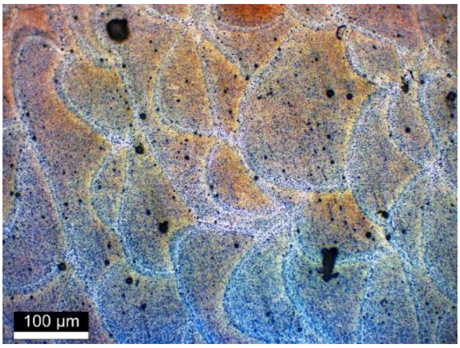

Fig. 8. Microstructure of a specimen with energy density, 49.9 J/mm^3 and 60° orientation

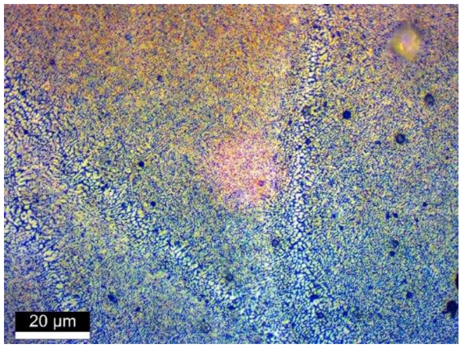

Fig. 9. Microstructure of a specimen shown in Fig. 8, depicting a columnar structure

A very high reduction in heat affected zone can be seen in Fig. 10 for the specimen with 60° orientation. This is attributed to optimum laser fusion of powders during melting. Again this aspect of the microstructure is demonstrated in Fig. 11, showing almost the absence of any columnar structure, but with porosity.

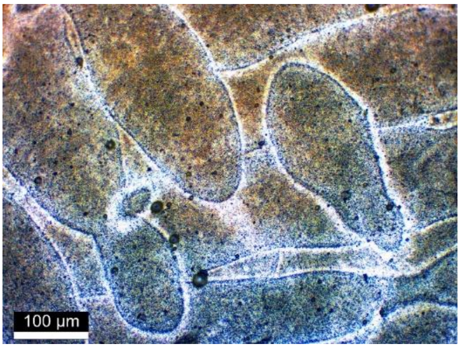

Fig. 10. Microstructure of a specimen with energy density, 49.9 J/mm^3 and 90° orientation

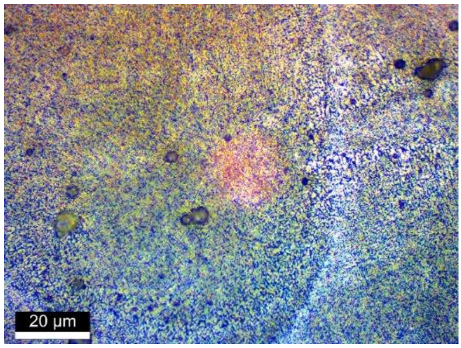

Fig. 11. Microstructure of a specimen shown in Fig. 10, with a columnar structure

Global Energy Density at 45.4 J/mm^3

The presence of melt pool boundaries with almost the absence of porosity is demonstrated in Fig. 12. and Fig. 13 shows a coarse columnar microstructure of the same specimen at another location.

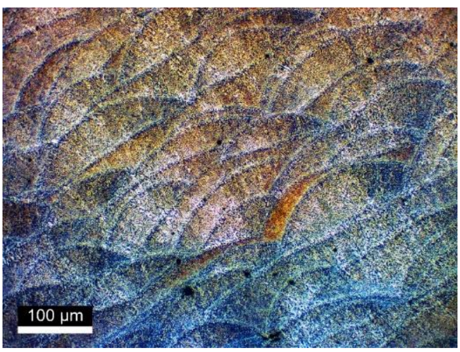

Fig. 12. Microstructure of a specimen with energy density, 45.4 J/mm^3 and 0° orientation

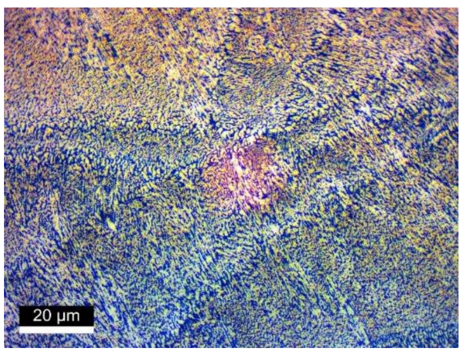

Fig. 13. Microstructure of a specimen shown in Fig. 12, reveals a coarse columnar structure

Fig. 14 shows the profile of melt pool boundaries suggesting the occurrence of better fusion between layers. Fig. 15 exhibits relatively a coarse columnar structure perhaps due to slower cooling rate at the boundaries between the fused layers.

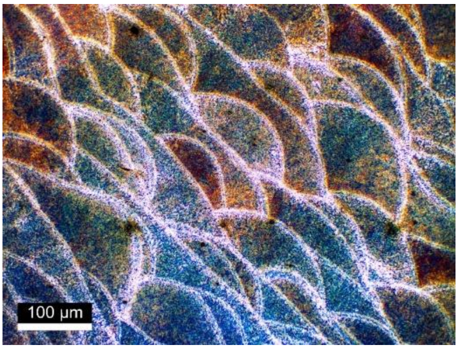

Fig. 14. Microstructure of a specimen with energy density, 45.4 J/mm^3 and 30° orientation

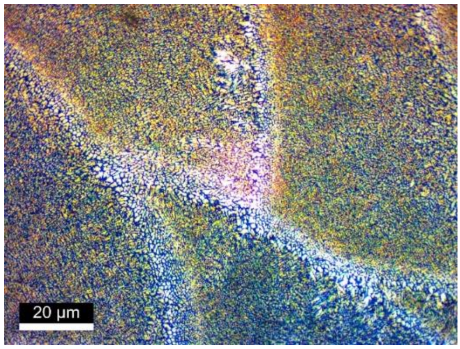

Fig. 15. Microstructure of a specimen shown in Fig. 14, but a coarse columnar structure

The microstructure of a 45^0 orientation specimen, as shown in Fig. 16, reveals a homogeneous microstructure but with porosity. Relatively higher amount of columnar growth can be seen in Fig. 17.

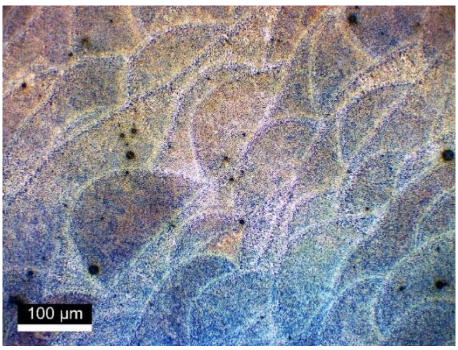

Fig. 16. Microstructure of a specimen with energy density, 45.4 J/mm^3 and 45° orientation

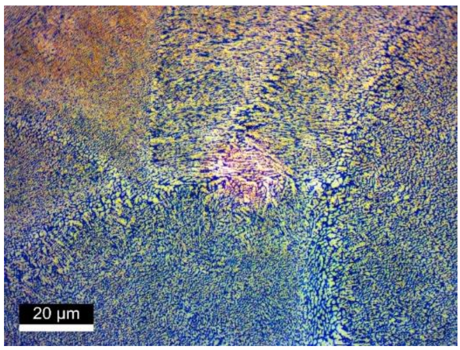

Fig. 17. Microstructure of a specimen shown in Fig. 16, with a coarse columnar structure

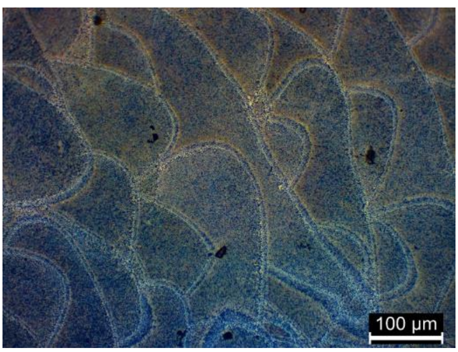

Fig. 18. Microstructure of a specimen with energy density, 45.4 J/mm^3 and 60° orientation

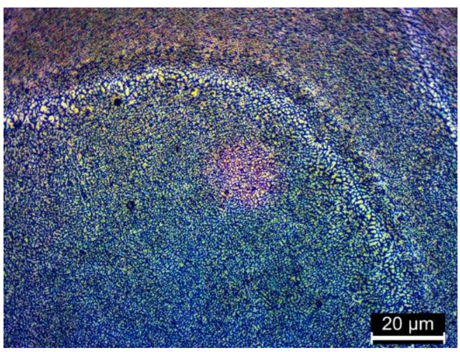

Fig. 19. Microstructure of a specimen shown in Fig. 18, with a coarse columnar structure along the melt pool boundaries

For the 60^0 orientation specimens, relatively modest level of porosity with melt pool boundaries are shown in Fig. 18. A very coarse columnar structure can be seen in Fig. 19, especially along the fused layers.

For the 90° orientation specimens, as shown in Fig. 20, higher amount of porosity, due to slower cooling rate, can be seen. Fig. 21 shows the widely affected regions of melt pool boundaries.

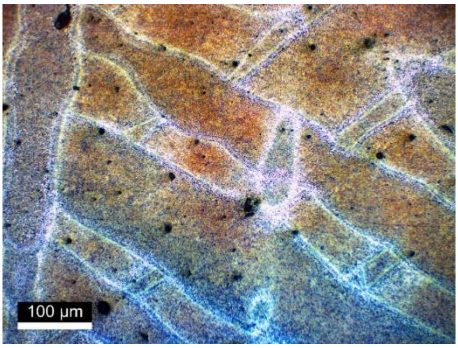

Fig. 20. Microstructure of a specimen with energy density, 45.4 J/mm^3 and 90° orientation

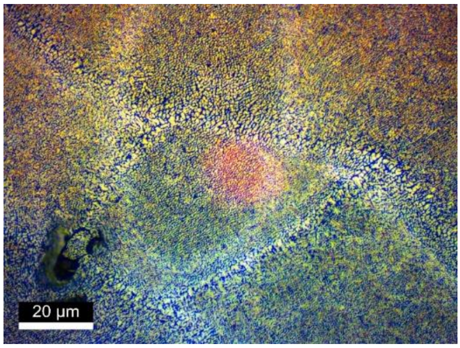

Fig. 21. Microstructure of a specimen shown in Fig. 20, with a highly affected melt pool boundaries

Global Energy Density at 37.1 J/mm^3

Fig. 22 reveals a microstructure with moderately fused layers (melt pool boundaries) showing the absence of porosity. Relatively a large heat affected zone with a coarse columnar structure is demonstrated in Fig. 23.

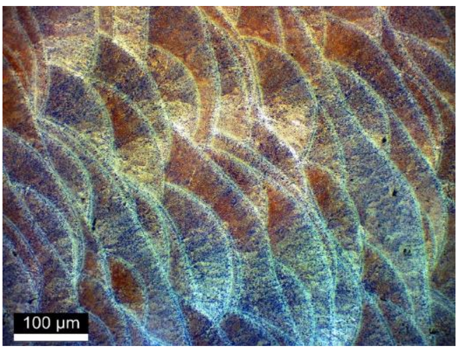

Fig. 22. Microstructure of a specimen with energy density, 37.1 J/mm^3 and 0° orientation

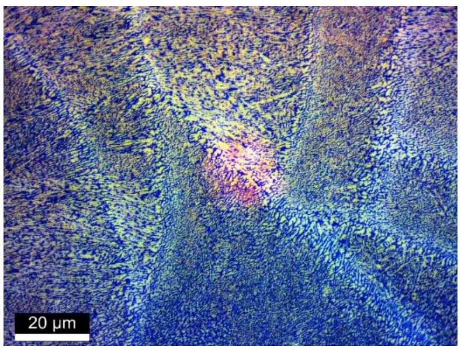

Fig. 23. Microstructure of a specimen shown in Fig. 22, with a coarse columnar structure

Reduced levels of porosity and coarse columnar structure are demonstrated in Fig. 24 and Fig. 25, respectively.

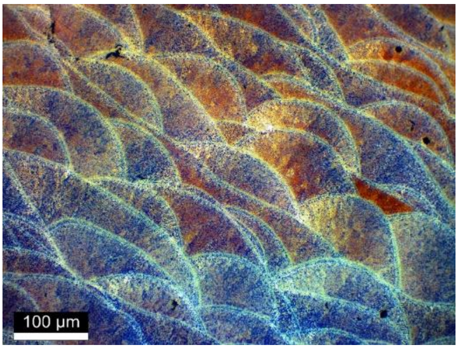

Fig. 24. Microstructure of a specimen with energy density, 37.1 J/mm^3 and 30° orientation

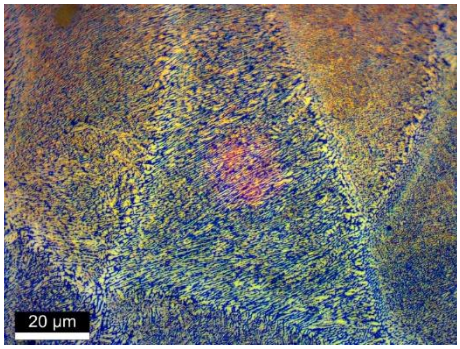

Fig. 25. Microstructure of a specimen shown in Fig. 24, with a coarse columnar structure

Fig. 26 reveals the presence of porosity at isolated locations closer to the fused layers. Relatively finer columnar structure is exhibited in Fig. 27.

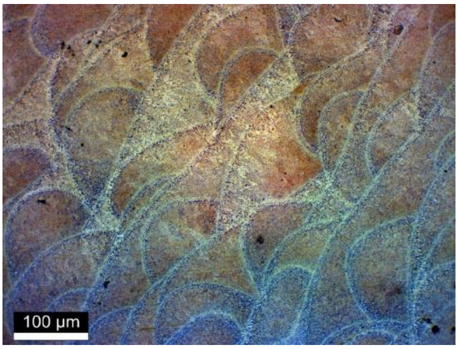

Fig. 26. Microstructure of a specimen with energy density, 37.1 J/mm^3 and 45° orientation

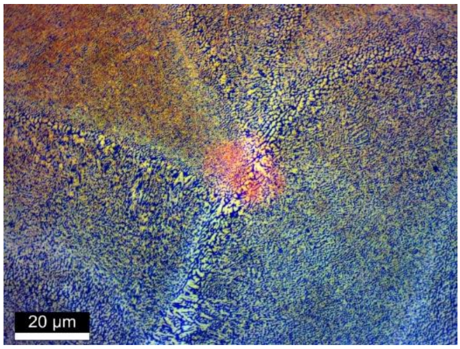

Fig. 27. Microstructure of a specimen shown in Fig. 26, with relatively a finer columnar structure

Fig. 28 shows the merging of fused layers as a result of insufficient hatch spacing. The presence of columnar structure and porosity is revealed in Fig. 29.

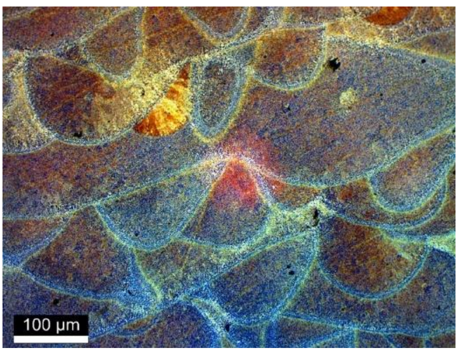

Fig. 28. Microstructure of a specimen with energy density, 37.1 J/mm^3 and 60° orientation

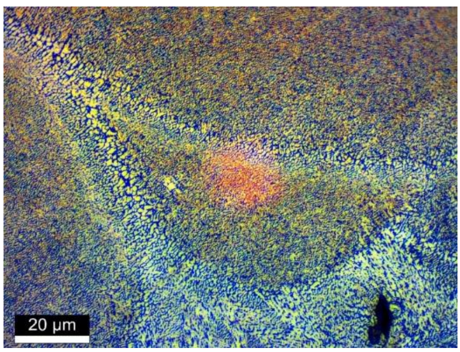

Fig. 29. Microstructure of a specimen shown in Fig. 28, with porosity and a columnar structure

Fig. 30 shows relatively a higher level of porosity and incomplete fused layers possibly due to low laser power used. Fig. 31 reveals higher levels of columnar growth and heat affected regions.

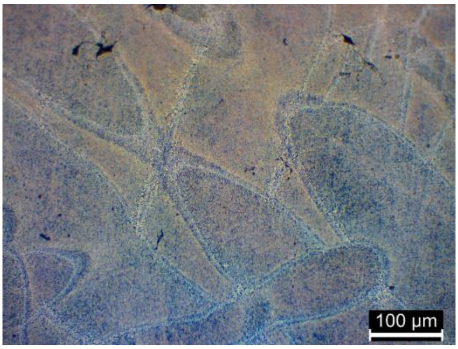

Fig. 30. Microstructure of a specimen with energy density, 37.1 J/mm^3 and 90° orientation

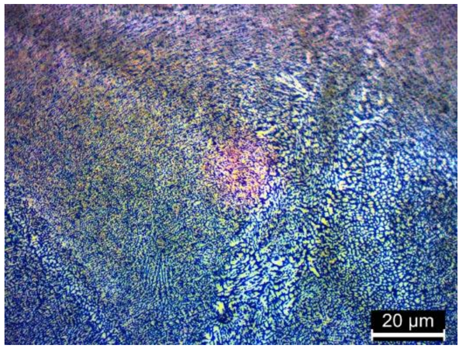

Fig. 31. Microstructure of a specimen shown in Fig. 30, with lots of columnar structure

As-built microstructures of the additive manufactured aluminum alloy samples/components are known to be very complex with fused layers of the metal powders. This is attributed mainly to the faster cooling rates during laser additive manufacturing [23, 24]. It has already been reported [25] that the specimen build angle orientations have a huge effect on the resulting columnar structures. Processing parameters, especially the laser power and the scan speed, have been reported [26] to influence the formation of porosity in the finished product. By controlling the heat input/diffusion rates at fused layer zones, homogeneous microstructure with finer columnar structure can be obtained [27].

Conclusions

Microscopy studies revealed optimal microstructures for energy densities at 45.4 J/mm^3 (with 0° orientation) and at 49.9 J/mm^3 (with 45° orientation) showing minimal porosity.

Aluminum alloy specimens with energy density 49.9 J/mm^3 produced relatively lesser heat affected zones and columnar structures.

Specimens with energy density at 37.1 J/mm^3 resulted mostly in inhomogeneous microstructure exhibiting coarse columnar structures.

With regard to the build angle orientations, the 90° build angle demonstrated almost no heat affected zone indicative of optimum fusion between metal powder layers.

Acknowledgement

Research was sponsored by the Army Research Laboratory and was accomplished under Cooperative Agreement Number W911NF-15-2-0020. The views and conclusions contained in this document are those of the authors and should not be interpreted as representing the official policies, either expressed or implied, of the Army Research Laboratory or the U.S. Government. The U.S. Government is authorized to reproduce and distribute reprints for Government purposes notwithstanding any copyright notation herein.

Thanks are also due to Mr. Gary Wyss, Senior Scientist, CAMP, for SEM analysis, Ronda Coguill, Taylor Winsor for the support on tensile test specimens, and Dr. Bruce Madigan.

References

[1] E. O. Olakanmi, R. F. Cochrane and K. W. Dalgrno, *A review on selective laser sintering/melting (SLS/SLM) of aluminum alloy powders: Processing, microstructure, and properties*, **Progress in Materials Science**, 2015, pp. 401-477.

[2] D. Buchbinder, W. Meiners, K. Wissenbach and R. Popraw, *Selective laser melting of aluminum die-cast alloy - Correlations between process parameters, solidification conditions, and resulting mechanical properties*, **Journal of Laser Applications**, 2015, pp. S29205-1-S29205-6.

[3] D. Herzog, V. Seyda, E. Wycisk and C. Emmelmann, *Additive manufacturing of metals*, **Acta Materialia**, pp. 371-392, 2016.

[4] N. T. Aboulkhair, I. Maskery, C. Tuck, I. Ashcroft and N. M. Everitt, *Improving the fatigue behaviour of a selectively laser melted aluminum alloy: Influence of heat treatment and surface quality*, **Materials and Design**, 2016, pp. 174-182.

[5] N. T. Aboulkhair, I. Maskery, C. Tuck, I. Ashcroft and N. M. Everitt, *The microstructure and mechanical properites of selectively laser melted AlSi10Mg: The effect of a conventional T6-like heat treatment*, **Materials Science and Engineering A**, 2016, pp. 139-146.

[6] N. T. Aboulkhair, N. M. Everitt, I. Ashcroft and C. Tuck, *Reducing porosity in AlSi10Mg parts processed by selective laser melting*, **Additive Manufacturing**, 2014, pp. 77-86.

[7] N. Read, W. Wang, K. Essa and M. M. Attallah, *Selective laser melting of AlSi10Mg alloy: Process optimisation and mechanical properties development*, **Materials and Design**, 2015, pp. 417-424.

[8] E. Brandl, U. Heckenberger, V. Holzinger and D. Buchbinder, *Additive manufactured AlSi10Mg samples using Selective Laser Melting (SLM): Microstructure, high cycle fatigue, and fracture behavior*, **Materials and Design**, 2012, pp. 159-169.

[9] J. Wu, X. Q. Wang, M. M. Attallah and M. H. Loretto, *Microstructure and strength of selectively laser melted AlSi10Mg*, **Acta Materialia**, 2016, pp. 311-320.

[10] I. Rosenthal, A. Stern and N. Frage, *Microstructure and Mechanical Properties of AlSi10Mg Parts Produced by the Laser Beam Additive Manufacturing (AM) Technology*, **Metallography, Microstructure and Analysis**, 2014, pp. 448-453.

[11] W. Li, S. Li, J. Liu, A. Zhang, Y. Zhou, Q. Wei, C. Yan and Y. Shi, *Effect of heat treatment on AlSi10Mg alloy fabricated by selective laser melting: Microstructure evolution, mechanical properties, and fracture mechanism*, **Materials Science & Engineering A**, 2016, pp. 116-125.

[12] R. Chou, A. Ghosh, S. C. Chou, M. Paliwal and M. Brochu, *Microstructure and mechanical properties of Al10SiMg fabricated by pulsed laser powder bed fusion*, **Materials Science & Engineering A**, 2017, pp. 53-62.

[13] U. Tradowsky, J. White, R. M. Ward, N. Read, W. Reimers and M. M. Attallah, *Selective laser melting of AlSi10Mg Influence of post-processing on the microstructural and tensile properties development*, **Materials and Design**, 2016, pp. 212-222.

[14] M. Tang and C. Pistorius, *Oxides, porosity and fatigue performance of AlSi10Mg parts produced by selective laser melting*, **International Journal of Fatigue**, 2017, pp. 192.

[15] N. Takata, H. Kodaira, K. Sekizawa, A. Suzuki and M. Kobashi, *Change in microstructure of selectively laser melted AlSi10Mg alloy with*, **Materials Science & Engineering A**, 2017, pp. 218-228.

[16] W. Pei, W. Zhengying, C. Zhen, D. Jun, H. Yuyang, L. Junfeng and Z. Yatong, *The AlSi10Mg samples produced by selective laser melting: single track, densification, microstructure and mechanical behavior*, **Applied Surface Science**, 2017, pp. 38-50.

[17] Y. J. Liu, Z. Liu, Y. Jiang, G. W. Wang, Y. Yang and L. C. Zhang, *Gradient in microstructure and mechanical property of selective laser melted AlSi10Mg*, **Journal of Alloys and Compounds**, 2018, pp. 1414-1421.

[18] D. Dai, D. Gu, H. Zhang, J. Xiong, C. Ma, C. Hong and R. Popraw, *Influence of scan strategy and molten pool configuration on microstructures and tensile properties of selective laser melting additive manufactured aluminum based parts*, **Optics and laser Technology**, 2018, pp. 91-100.

[19] S. Liu, H. Zhu, G. Peng, J. Yin and Z. Xiaoyan, *Microstructure prediction of selective laser melting AlSi10Mg using finite element analysis*, **Materials & Design**, 142, 2017, pp. 319-328.

[20] N. Takata, H. Kodaira, A. Suzuki and M. Kobashi, *Size dependence of microstructure of AlSi10Mg alloy fabricated by selective laser melting*, **Materials Characteriazation**, 2017, DOI: 10. 1016/j. matchar. 2017. 11. 052.

[21] L. J. Suttey, *Evaluation of Metallurgical and Mechanical Properties of AlSi10Mg Produced by Selective Laser Melting*, **https://digitalcommons. mtech. edu**/grad_rsch/174, 2018, pp. 1-98.

[22] K. G. Prashanth, S. Scudino, H. J. Klauss, K. B. Surreddi, L. Löber, Z. Wang, A. K. Chaubey, U. Kühn and J. Eckert, *Microstructure and mechanical properties of Al-12Si produced by selective laser melting: Effect of heat treatment*, **Materials Science & Engineering A**, 590, 2014, pp. 153-160.

[23] I. Maskery, N. T. Aboulkhair, M. R. Corfield, C. Tuck, C. Clare, R. K. Leach, R. D. Wildman, I. A. Ashcroft and R. J. Hague, *Quantification and characterisation of porosity in selectively laser melted Al-Si10-Mg using X-ray computed tomography*, **Materials Characterization**, 111, 2016, pp. 193-204.

[24] D. Herzog, V. Seyda, E. Wycisk and C. Emmelmann, *Addivie manufacturing of metals*, **Acta Materialia**, 2016, pp. 371-392.

[25] N. T. Aboulkhair, N. M. Everitt, I. Ashcroft and C. Tuck, *Reducing porosity in AlSi10Mg parts processed by selective laser melting*, **Additive Manufacturing**, 2014, pp. 77-86.

[26] C. Weingarten, D. Buchbinder, N. Pirch, W. Meiners, K. Wissenbach and R. Poprawe, *Formation and reduction of hydrogen porosity during selective laser melting of AlSi10Mg*, **Journal of Materials Processing Technology**, 2015, pp. 112-120.

Received: November 6, 2018
Accepted: December 10, 2018